scientific reports

Check for updates

OPEN

High-resolution ultrasound imaging of the spinal accessory nerve and associated injuries based on a prospective normative study and retrospective analysis

Zijian Tai[1,4], Lihua Liu[2,4], Tiezheng Wang[2], Yeting Wang[3], Kezhen Qin[3], Wen Chen[3], Huawei Zhang[2] & Hengtao Qi[2]✉

This study assessed the feasibility of high-resolution ultrasound (HRUS) for visualizing the cervical spinal accessory nerve (SAN) and explored its sonographic characteristics, anatomical landmarks, and normative diameter measurements. A prospective study was conducted in 60 healthy volunteers, in whom the SAN was categorized into three segments: between the trapezius and levator scapulae (S1), from the surface of the levator scapulae to the posterior border of the sternocleidomastoid muscle (SCM) (S2), and from the posterior border of the SCM to the upper cervical region (S3). HRUS was utilized to evaluate SAN visibility and measure the maximum short-axis diameter (SD), with normative values statistically analyzed. In addition, a retrospective analysis was performed in 12 patients with clinically and electrophysiologically confirmed SAN injury to characterize sonographic abnormalities. HRUS successfully delineated the SAN and adjacent structures with a 100% visibility rate across all segments. No significant differences in SD were observed between sides, segments, or sexes, though SD exhibited a positive correlation with body mass index (BMI). In patients with SAN injury, HRUS identified complete nerve rupture, with all cases presenting trapezius muscle atrophy. These findings establish HRUS as a reliable, non-invasive imaging modality for assessing SAN morphology and diagnosing nerve injuries.

Keywords Accessory nerve, Ultrasonography, Peripheral nerve injuries, Brachial plexus neuropathies, Diagnostic imaging

Abbreviations

SAN	Spinal accessory nerve
SCM	Sternocleidomastoid muscle
TM	Trapezius muscle
LS	Levator scapulae muscle
GAN	Great auricular nerve
SCN	Supraclavicular nerve
TN	Traumatic neuroma
HRUS	High-resolution ultrasound
SD	Short-axis diameter
BMI	Body mass index
ANOVA	Analysis of variance
ICC	Intraclass correlation coefficient
MRI	Magnetic resonance imaging
CT	Computed tomography

[1]Shandong Provincial Hospital, Shandong University, Jinan, Shandong, China. [2]Department of Ultrasound, Shandong Provincial Hospital Affiliated to Shandong First Medical University, No.324, Jingwu Road, Jinan 250021, Shandong, China. [3]Shandong First Medical University, No.6699, Qingdao Road, Jinan 250117, Shandong, China. [4]Zijian Tai and Lihua Liu: Co-first authors. ✉email: elementfe@126.com

SPSS Statistical Package for the Social Sciences

The spinal accessory nerve (SAN) traverses from the base of the skull through the jugular foramen into the neck, coursing anterolateral to the internal jugular vein, deep to the posterior belly of the digastric muscle, and the stylohyoid muscle. It continues deep to the sternocleidomastoid muscle (SCM) and enters the posterior cervical triangle at its posterior edge, then runs superficially over the levator scapulae muscle before entering the deep surface of the trapezius muscle at the junction of its middle and lower thirds, where it branches to innervate the trapezius muscle[1]. Nevertheless, its anatomical course also exhibits various variations[2,3], and a recent study identified a rare dual SAN variation[4]. In the posterior cervical triangle, the SAN is relatively superficial and closely associated with lymph nodes, making it susceptible to iatrogenic injury during radical neck dissection and cervical lymph node biopsy[5–7]. Additionally, SAN injury has been reported during procedures such as internal jugular vein puncture, thyroidectomy, carotid endarterectomy[8], neck trauma, cervicofacial lifting[9,10], and even following neck stretching or deep massage[11]. The proposed mechanisms of injury include compression[12,13], traction[10], thermal injury, and direct severance[14]. The SAN is a motor cranial nerve that innervates the SCM, trapezius, and pharyngeal muscles. Cervical SAN injury can lead to restricted shoulder abduction, shoulder drooping, and scapular winging. Iatrogenic SAN injury is a significant cause of medical malpractice litigation. Therefore, early diagnosis and appropriate management of SAN injuries are crucial to prevent long-term complications.

Traditional diagnostic methods, including physical examination and nerve conduction studies, are helpful in evaluating and diagnosing SAN injury but are often limited in determining the exact location and extent of the damage. Thus, there is a need for a more precise and direct diagnostic tool to bridge this gap. The development of high-resolution ultrasound (HRUS) technology offers new possibilities for diagnosing SAN injuries. HRUS has the advantages of being non-invasive, providing real-time imaging, and offering high tissue resolution, making it ideal for identifying superficial structures and dynamically evaluating small nerves. Compared with conventional ultrasound, HRUS enables clearer visualization of peripheral nerves, including their fascicular and epineurial compartments, and allows microvascular mapping with high-frequency transducers, thereby improving diagnostic accuracy[15]. Therefore, HRUS is an excellent choice for assessing the SAN and its associated pathologies.

There is limited literature on the HRUS of the SAN and its injuries. This study aims to detail the scanning method for the cervical SAN, evaluate the visualization capability of HRUS in the cervical SAN of healthy volunteers, measure and statistically analyze the normal values of the SAN's short-axis diameter (SD), and summarize the HRUS characteristics of injured SANs. This study explores the potential application of HRUS in diagnosing SAN injuries, providing a more accurate and comprehensive diagnostic basis for clinical practice.

Materials and methods

Study approval

This study was approved by the ethics committee of Shandong Provincial Hospital Affiliated to Shandong First Medical University (No. MR-37–23-023,994). This study was conducted according to the principles outlined in the Declaration of Helsinki (as revised in 2013). All volunteers and patients provided written informed consent.

Ultrasound examination of healthy volunteers

This prospective study recruited 60 healthy volunteers from among our hospital's resident physicians and staff from January to May 2024. Inclusion criteria were volunteers older than 18 years of age. Exclusion criteria included myopathies, polyneuropathies, chronic diseases that may cause peripheral neuropathy, neck injuries, and a history of neck surgery. Basic information collected from the volunteers included age, sex, and body mass index (BMI).

All ultrasound examinations were conducted utilizing the Canon Aplio i800 and GE LOGIQ E11 ultrasound systems. These systems were equipped with high-frequency linear probes (24 MHz for the Aplio i800 and 20 MHz for the LOGIQ E11), and examinations were performed under superficial musculoskeletal examination conditions, with depth 1.5–3.0 cm and a single focal zone placed at or just below the SAN. Compound and tissue harmonic imaging were enabled; overall gain/dynamic range were adjusted to optimize nerve–soft-tissue contrast, and speckle reduction kept low. The probe was maintained perpendicular to the nerve with minimal pressure to limit anisotropy, and both short- and long-axis planes were obtained. Two radiologists with over 10 years of experience in musculoskeletal ultrasound independently conducted the examinations on the bilateral cervical SAN of the volunteers.

The cervical SAN was divided into three segments for the ultrasound examination: the first segment (S1) was between the trapezius and levator scapulae muscles; the second segment (S2) was from the surface of the levator scapulae to the posterior edge of the SCM or the posterior cervical triangle; and the third segment (S3) was from the posterior edge of the SCM to the upper neck.

Ultrasound examination method

The subjects were placed in a supine position with slight neck extension during the ultrasound examination. The probe was initially placed vertically on the mid-clavicle and moved upwards to display the trapezius muscle at the shoulder. The deeper structure of the trapezius muscle was the levator scapulae muscle. At the middle and lower thirds of the anterior edge of the trapezius, the cross-section of the SAN was identified. After identifying the SAN with ultrasound, the probe was moved along the neck where the SAN runs on the surface of the levator scapulae muscle. The probe was then moved superiorly along the SAN into the SCM until the SAN could no longer be visualized. Color Doppler ultrasound was used during the examination to differentiate the SAN from small blood vessels. Key aspects to focus on during the ultrasound examination included: (1) the visibility rate

of the SAN in the three segments; (2) the anatomical relationship of the SAN; and (3) the maximum SD of the SAN measured in the three segments. The probe was maintained at a perpendicular angle to the nerve during measurements. To improve reproducibility, a standardized scanning protocol for cervical peripheral nerves was followed, as recommended in previous literature[16–18].

Ultrasound examination of patients

This retrospective study included patients with suspected SAN lesions at our hospital from July 2021 to October 2024. Suspicion of SAN injury was defined when ≥ 2 of the following were present: (1) relevant history-recent neck surgery/biopsy or interventions at cervical levels II–V or cervical trauma; (2) characteristic symptoms-shoulder droop/asymmetry, shoulder-shrug weakness, reduced active abduction, scapular dyskinesis, or shoulder-girdle pain; (3) examination findings—trapezius atrophy/asymmetry, shoulder-shrug strength ≤ 4/5, lateral scapular winging, or reduced upward rotation. When available, supportive evidence included electrodiagnostics or prior imaging suggestive of SAN pathology. Patients were excluded when alternative etiologies were more likely. All patients had unilateral lesions and underwent HRUS examination following the scanning method described above to identify SAN injuries, such as nerve thickening, echo interruption, and traumatic neuromas. Ultrasound examinations were conducted using the Canon Aplio i800 and GE LOGIQ E11 systems, each equipped with linear array probes of 24 MHz and 20 MHz, respectively. The HRUS characteristics of the damaged accessory nerve were observed and compared with the healthy side.

Statistical analysis

All statistical analyses were performed using SPSS software, version 29.0 (IBM Corp., Armonk, NY, USA). Continuous variables were tested for normality using the Shapiro–Wilk test. Data are presented as mean ± standard deviation and range. Comparisons of SAN SD among the three anatomical segments (S1–S3) were performed using one-way analysis of variance (ANOVA), followed by the Student–Newman–Keuls post hoc test. Differences between male and female subjects were analyzed using the independent samples t-test, and left–right side differences were evaluated with the paired t-test. Associations between SAN SD and BMI were assessed using Pearson's correlation coefficient. Intraobserver reliability of repeated measurements was evaluated using the intraclass correlation coefficient (ICC, two-way mixed model, absolute agreement, single measurement). All statistical tests were two-sided, and a P value < 0.05 was considered statistically significant. Ninety-five percent confidence intervals (95% CI) were reported where applicable to provide estimates of precision.

Results

A total of 60 healthy volunteers (28 males and 32 females) were recruited for this study, with an average age of 36.58 ± 7.67 years (age range: 20–59 years). HRUS examination of the cervical SAN in healthy adults revealed three segments: S1, the segment between the trapezius and levator scapulae muscles (Fig. 1); S2, from the surface of the levator scapulae to the posterior edge of the SCM, also known as the posterior cervical triangle (Fig. 2); and S3, from the posterior edge of the SCM to the upper neck, where the great auricular nerve could be seen running along the surface of the SCM and the supraclavicular nerve could be seen running medially to the SAN, extending posteriorly and inferiorly (Fig. 3). In the short-axis view, the normal SAN consistently exhibited a monofascicular appearance, seen as a single, well-circumscribed hypoechoic focus ("single black dot/ball") surrounded by a thin hyperechoic epineurial rim, in contrast to the honeycomb pattern typically observed in polyfascicular peripheral nerves. In the long-axis view, it appeared as a hypoechoic band without the multilobulated fascicular texture of polyfascicular nerves. Color Doppler ultrasound helped differentiate the SAN from adjacent small vessels and was applied routinely at S1 to exclude the superficial branch of the transverse cervical artery, which may mimic a small anechoic "black dot" on cross-Sects. [19]. The visibility rate of the cervical SAN in the 60 volunteers was 100% (120/120) for both sides and 100% (120/120) for each segment (S1, S2, and S3). In segment S3, ultrasound could only show the portion of the SAN from the posterior edge to the anterior edge of the SCM, as the complex anatomical structures and deeper location of the SAN between the anterior edge of the SCM and the base of the skull limited complete visualization.

The mean SDs of the SAN in segments S1, S2, and S3 were 0.61 ± 0.05 mm, 0.62 ± 0.07 mm, and 0.62 ± 0.01 mm, respectively, with no significant differences among the segments (Fig. 4A). There were no significant differences in the SDs of the SAN between the left and right sides (Table 1, Fig. 4B), or between males and females (Table 2, Fig. 4C). Pearson correlation analysis revealed a positive correlation between SAN SD and BMI, with a correlation coefficient of $r_{BMI} = 0.538$ ($P < 0.001$).

From July 2022 to March 2024, 12 patients were diagnosed with SAN injury through HRUS, confirmed by surgery or MRI. All patients had a history of neck surgery or trauma, including 7 cases of cervical lymph node biopsy, 3 cases of vascular anomaly surgery, and 2 cases of knife injury. Among these, 5 injuries were in segment S3, and 7 were in segment S2. Pathologic SANs showed characteristic changes: diffusely increased intraneural echogenicity consistent with neural fibrosis (the so-called "white nerve"), loss of normal fascicular definition, and caliber alterations. In cases with discontinuity, HRUS demonstrated complete nerve rupture with retracted proximal/distal stumps and bulbous traumatic neuroma at the ends in some patients, often accompanied by trapezius muscle atrophy and increased echogenicity of the affected muscle (Figs. 5, 6, Supplementary Video S1 and Supplementary Video S2). All 12 patients underwent surgical treatment.

Discussion

Cervical SAN injury can result in trapezius muscle weakness, leading to reduced shoulder abduction strength, chronic shoulder pain, deformity, and even persistent disability[7]. However, Camp SJ et al. found an average delay

A

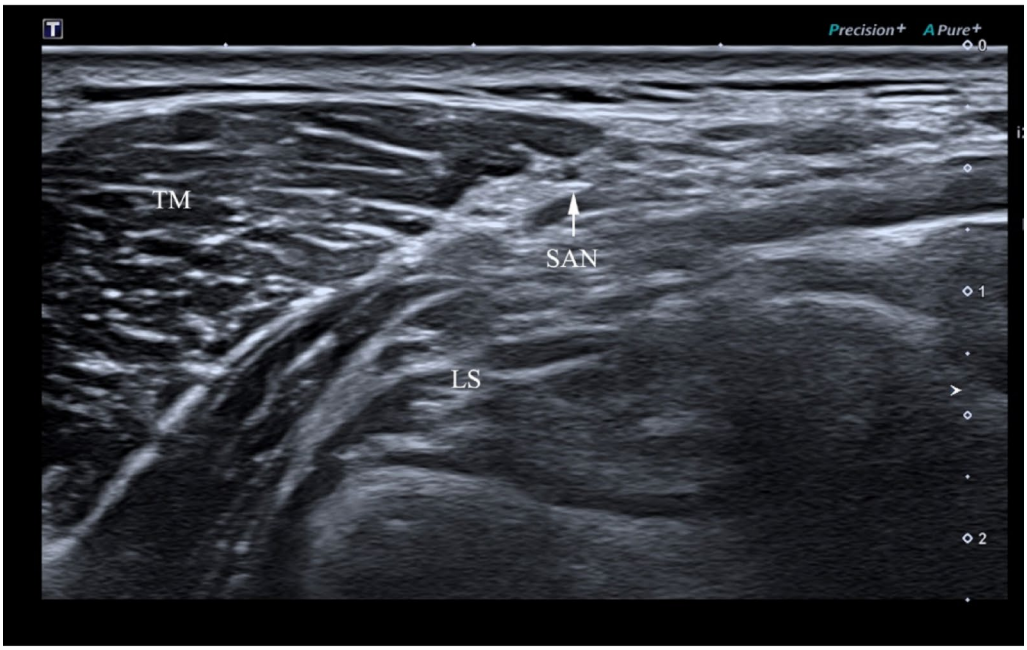

B

Fig. 1. Identifying the short axis of the spinal accessory nerve (SAN) at S1. **A** The spinal accessory nerve(arrow) runs between the trapezius (TM) and levator scapulae (LS). **B** Transducer placement is demonstrated.

of one year between SAN injury and diagnosis, which can lead to worse outcomes[14]. Therefore, timely evaluation of SAN injury is crucial to determine the need for surgical intervention and improve prognosis.

Electrophysiological studies are the most sensitive method for detecting nerve conduction disorders in SAN injury but cannot provide specific information about nerve structure or the location of the injury. Laughlin et al. reported the presence of spontaneous motor unit potentials on electromyography and low but present amplitudes in nerve conduction studies in patients with completely severed SANs[20], questioning the accuracy of electrophysiological studies in showing nerve continuity, especially considering that the trapezius muscle may also receive innervation from the cervical plexus.

Due to the small size of the cervical SAN, imaging techniques like CT and MRI are limited by resolution and real-time capability, making real-time dynamic observation and tracking challenging. Garrett et al. found

A

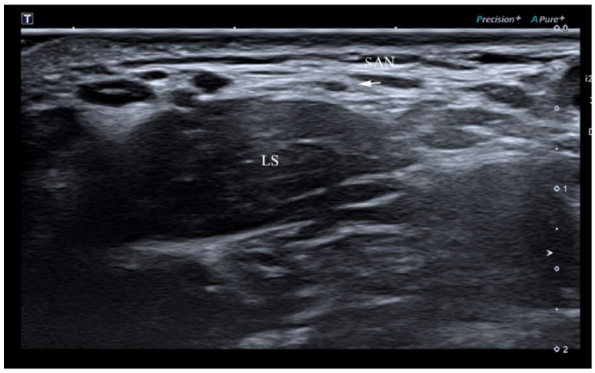

B

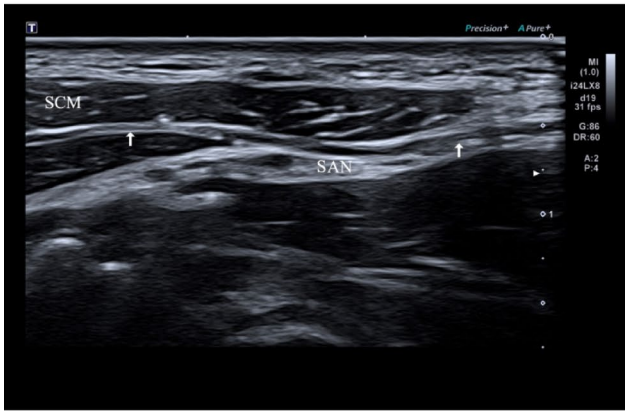

C

Fig. 2. Identifying the spinal accessory nerve (SAN) at S2. **A** Short-axis and **B** long-axis ultrasonographic views show the SAN (arrows) coursing on the surface of the levator scapulae (LS) within the posterior cervical triangle; the adjacent sternocleidomastoid muscle (SCM) is shown for orientation. **C** Transducer placement for the short-axis view.

A

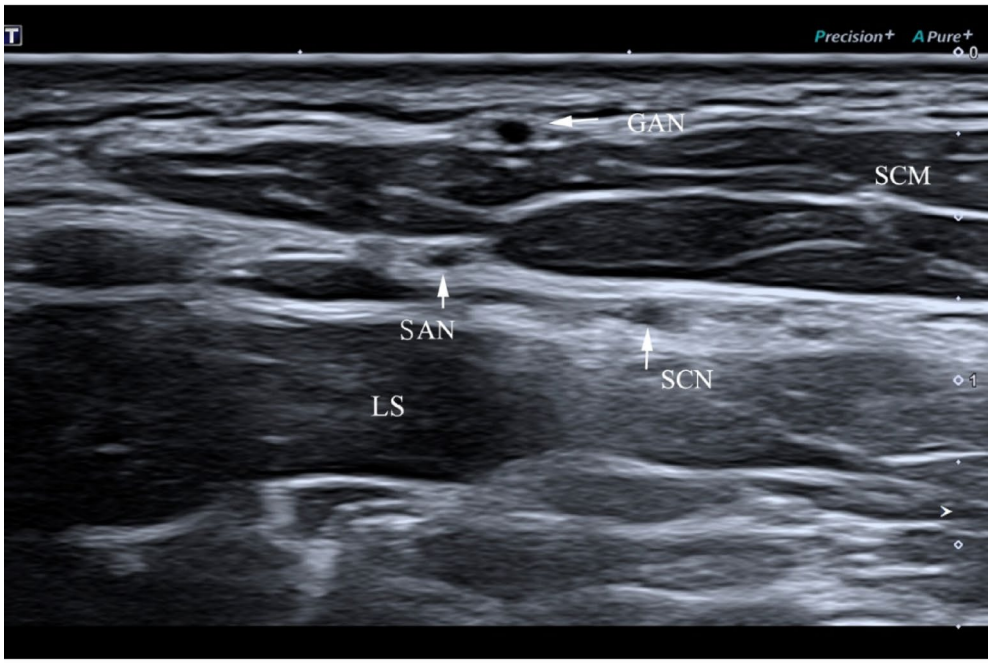

B

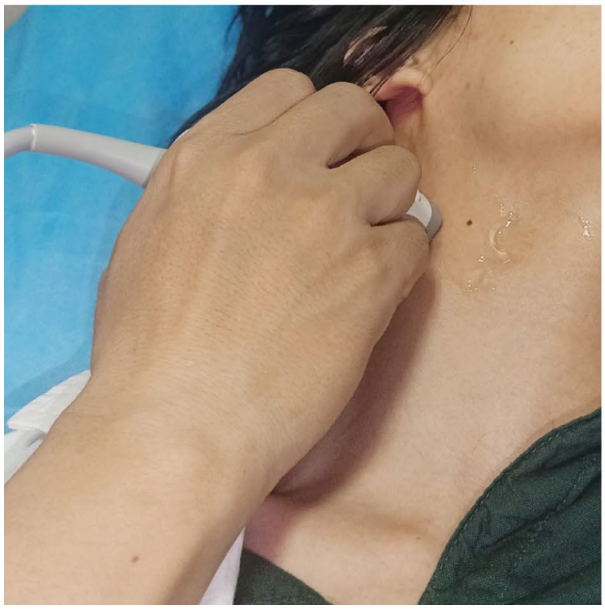

Fig. 3. Identifying the short axis of the spinal accessory nerve (SAN) at S3. **A** Short-axis ultrasound at S3 shows the SAN (arrow) posterior to the sternocleidomastoid muscle (SCM) and superficial to the levator scapulae (LS); the great auricular nerve (GAN, arrow) runs along the SCM surface, and the supraclavicular nerve (SCN, arrow) courses medial to the SAN, extending posterior–inferiorly over the LS. **B** Transducer placement is demonstrated.

that MRI could only visualize SAN injury in 24% of cases in a retrospective study of 38 patients[6]. High-field strength (3T or higher) scans and surface array coil imaging from the skull base to the axilla may improve SAN visualization.

HRUS is considered an effective imaging method for evaluating peripheral nerve lesions. With improved HRUS imaging quality, even small peripheral nerves with diameters of < 1.5–2 mm can be clearly visualized[21]. Previous studies have included some ultrasound research on the cervical SAN. Canella et al. observed that ultrasound could clearly display the SAN in the posterior cervical triangle in a study of 7 cadavers and 15 healthy

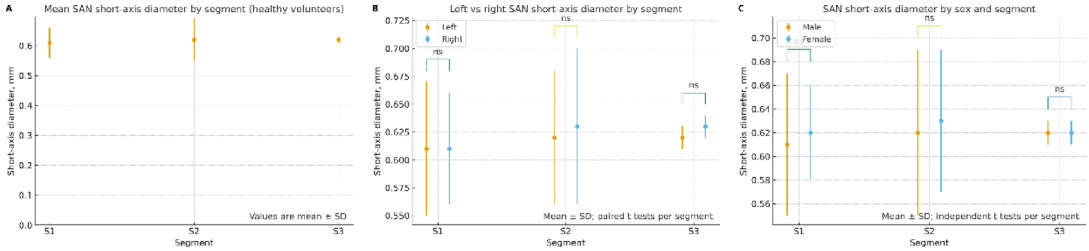

Fig. 4. Spinal accessory nerve (SAN) short-axis diameter (SD) in healthy volunteers and subgroup comparisons. **A** Mean SAN SD by segment (S1–S3), shown as mean ± SD; no significant among-segment differences (ANOVA, $P > 0.05$). **B** Left–right comparisons by segment, mean ± SD; no significant side-to-side differences (paired t tests, all $P > 0.05$; "ns" indicates not significant). C. Sex comparisons by segment, mean ± SD; no significant differences between males and females (independent samples t tests, all $P > 0.05$).

Variable	S1 (mm)	S2 (mm)	S3 (mm)
Left (60)	0.61 ± 0.06	0.62 ± 0.06	0.62 ± 0.01
Right (60)	0.61 ± 0.05	0.63 ± 0.07	0.63 ± 0.01
P value	0.906	0.461	0.446

Table 1. Short-axis diameter of cervical SAN between left and right sides. Data are presented as the mean ± SD. SAN, spinal accessory nerve; S1, between the trapezius and levator scapulae; S2, from the surface of the levator scapulae to the posterior edge of the sternocleidomastoid muscle, also known as the posterior cervical triangle; S3, from the posterior edge of the SCM to the upper neck.

Variable	S1 (mm)	S2 (mm)	S3 (mm)
Male (28)	0.61 ± 0.06	0.62 ± 0.07	0.62 ± 0.01
Female (32)	0.62 ± 0.04	0.63 ± 0.06	0.62 ± 0.01
P value	0.215	0.635	0.889

Table 2. Short-axis diameter of cervical SAN between male and female groups. Data are presented as the mean ± SD. SAN, spinal accessory nerve; S1, between the trapezius and levator scapulae; S2, from the surface of the levator scapulae to the posterior edge of the sternocleidomastoid muscle, also known as the posterior cervical triangle; S3, from the posterior edge of the SCM to the upper neck.

volunteers[22]. Hong et al. demonstrated that ultrasound could visualize the SAN in cervical lymph node levels II, III, IV, and V and suggested that ultrasound guidance could prevent SAN injury during neck surgery[23]. Casaletto et al. revealed that ultrasound had the same accuracy as MRI in diagnosing cervical SAN lesions and suggested that both ultrasound and MRI could be used as imaging methods for SAN pathology[24]. Sara et al. discovered that electrodiagnostic examination and HRUS detected abnormalities of the trapezius muscle and the SAN with comparable sensitivity and specificity[25]. Cesmebasi et al. reported a high positive predictive value of iatrogenic SAN transection with ultrasound[7].

This study examined the HRUS imaging characteristics of the cervical spinal accessory nerve and established normative reference values for its clinical application[26,27], which were largely concordant with prior research outcomes[28]. The study confirmed the feasibility of visualizing the SAN using HRUS, as the normal SAN could be observed in all volunteers. In HRUS, the SAN appeared hypoechoic, surrounded by echogenic connective tissue in both short-axis and long-axis views. On short-axis, the normal SAN demonstrated a single, well-circumscribed hypoechoic focus bordered by a thin hyperechoic rim, contrasting with the honeycomb texture of polyfascicular nerves; on long-axis, it appeared as a smooth hypoechoic band without multilobulated fascicles. Pathologically, increased intraneural echogenicity ("white nerve") was consistent with fibrosis and loss of fascicular definition and co-occurred with caliber change and discontinuity in injured cases. However, the complex anatomy and deeper location of the SAN between the skull base and the internal jugular vein limited complete visualization by ultrasound. From a practical standpoint, routine color/power Doppler at S1 is pivotal to avoid mistaking the superficial branch of the transverse cervical artery for the SAN when both may present as small "black dots." Statistical analysis of the measurements of the bilateral SAN showed no significant differences in the maximum diameter, consistent with previous reports of other peripheral nerves[29–32]. Therefore, comparing the morphology and measurements of the bilateral SAN can help identify abnormalities. The observed positive association between SAN diameter and BMI suggests that body habitus should be considered when interpreting borderline measurements, and that BMI-aware reference intervals may further refine diagnostic thresholds. Additionally, no significant differences were found among the segments, and SAN SD was correlated with BMI (rBMI = 0.670,

A

B

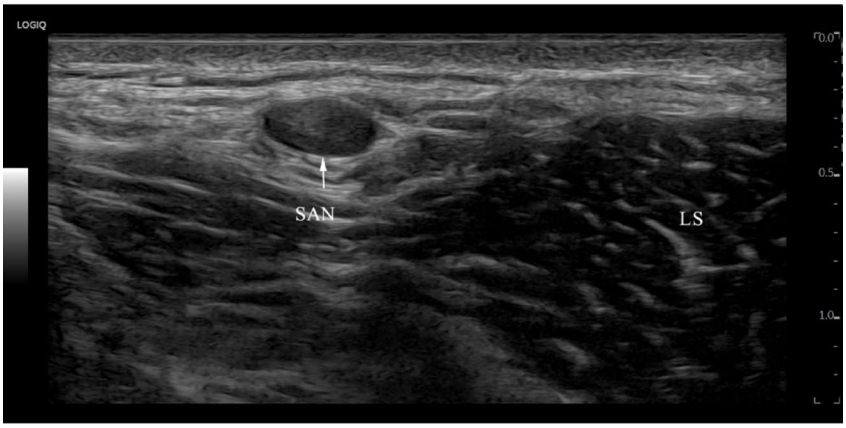

C

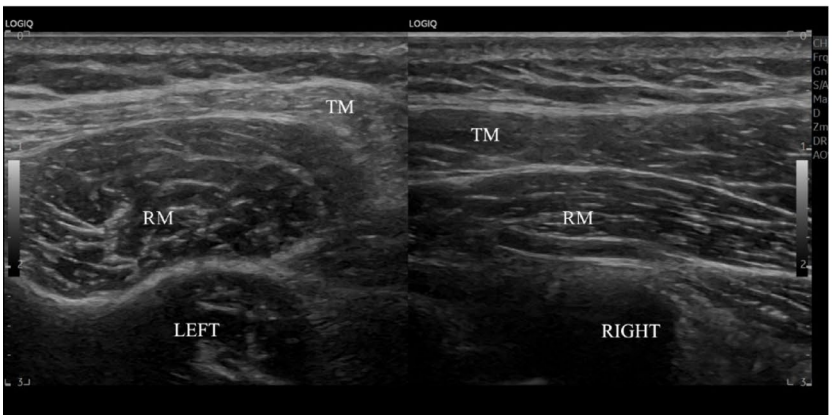

Fig. 5. A 42-year-old female presented with left shoulder elevation weakness six months after a lymph node biopsy. **A** A clinical photograph shows left shoulder drooping and winged scapula. **B** High-resolution ultrasound (short-axis) at S2 shows rupture of the spinal accessory nerve (SAN) with traumatic neuroma (TN) on the affected side; the nerve lies superficial to the levator scapulae (LS). **C** Ultrasound of the trapezius (TM) on the affected side demonstrates denervation atrophy (thinning and increased echogenicity), with the underlying Rhomboids (RM) labeled for orientation.

A

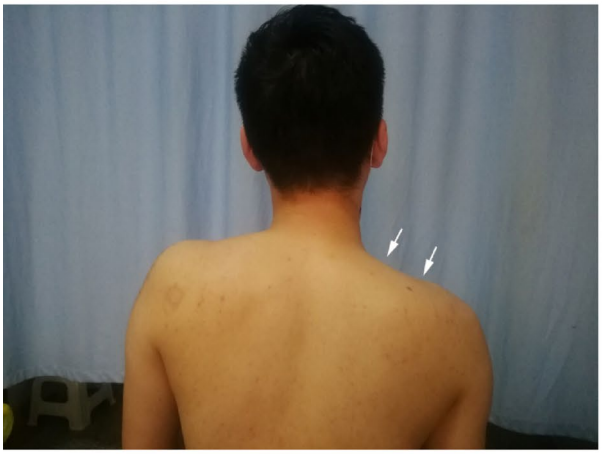

B

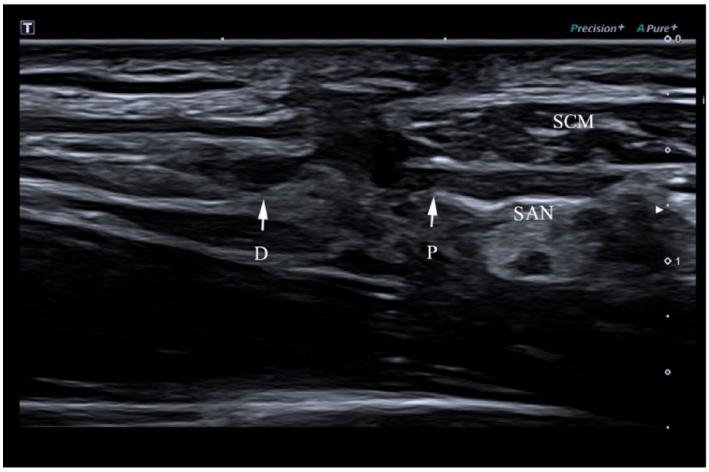

C

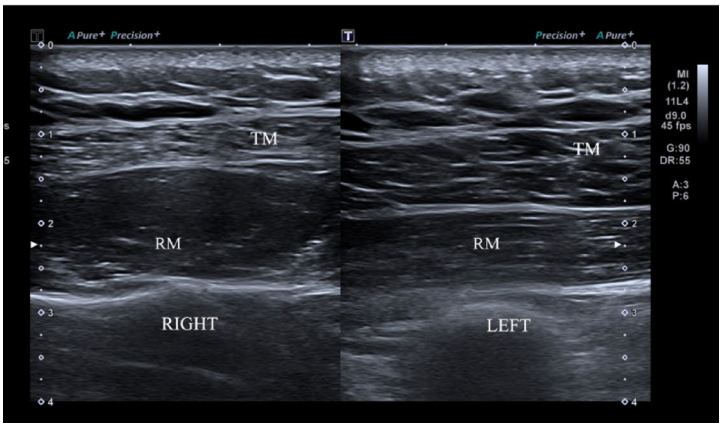

Fig. 6. A 33-year-old male complained of right shoulder pain, weakness, and numbness four months after a stab injury. **A** A clinical photograph demonstrates right shoulder drooping. **B** Ultrasonography shows complete transection of the spinal accessory nerve (SAN); P denotes the proximal stump and D the distal stump. The adjacent sternocleidomastoid muscle (SCM) exhibits focal fibrous disruption. **C** Ultrasound of the trapezius (TM) on the affected side demonstrates denervation atrophy (thinning and increased echogenicity), with the underlying Rhomboids (RM) labeled for orientation.

$P < 0.001$). The SD of the injured SAN in patients exceeded the normal range, and the study's data can serve as a reference for further evaluation of various SAN neuropathies.

All SAN neuropathies in this study occurred after neck surgery or trauma, consistent with previous reports[33–35]. In this study, 58% of SAN neuropathies were located in S2, where the SAN is relatively superficial and closely associated with lymph nodes, making it ideal for observation with HRUS. Overall, when SAN neuropathy is suspected, comparing the contralateral SAN can help identify abnormal nerve morphology or course. In 12 patients, the SAN was completely severed, with nerve ends showing thickening and neuroma-like swelling in some cases, making it difficult to distinguish nerve ends from surrounding scar tissue. Continuous scanning helps identify the location of nerve injury, and the patient's history and ultrasound findings of trapezius muscle atrophy prompt careful examination for SAN injury. Morphological evaluation with HRUS accurately diagnosed SAN neuropathy in all cases. Additionally, HRUS is useful for postoperative follow-up. The predominance of lesions in S2 is anatomically and surgically plausible and supports targeted protocols that prioritize the posterior cervical triangle during pre- and postoperative assessments.

HRUS should be incorporated early in the diagnostic pathway for suspected SAN injury. It enables rapid determination of continuity versus transection, precise lesion localization, and characterization of stump/neuroma configuration to inform operative strategy (direct repair vs. grafting). Concurrent documentation of trapezius involvement provides a structural substrate for symptoms and a baseline for postoperative surveillance. In elective neck procedures (e.g., lymph-node biopsy/dissection), preoperative HRUS mapping may aid risk stratification and intraoperative safeguarding.

This single-center study enrolled predominantly young to middle-aged adults, which may limit generalizability of normative values to adolescents and older adults. The patient cohort was relatively small and retrospectively accrued; longitudinal functional outcomes after intervention were not systematically captured. Interobserver agreement was not assessed. Quantification focused on maximum short-axis diameter rather than cross-sectional area, elastography, or quantitative echotexture. Future work should include multicenter prospective cohorts with age-diverse participants; expanded metrics (CSA, elastography, microvascular mapping); interobserver reliability; and evaluating thresholds that predict surgical benefit.

Conclusion

In this study, HRUS reliably visualized the cervical SAN in healthy volunteers and diagnosed SAN injuries in patients. HRUS allows clear observation of the cervical SAN and can be considered the preferred method for evaluating SAN injuries.

Data availability

The data that support the findings of this study are available from the authors, but restrictions apply to the availability of these data, which were used under license from the Shandong Provincial Hospital Affiliated to Shandong First Medical University for the current study, and so are not publicly available. Data are, however, available from the authors upon reasonable request and with permission from the Shandong Provincial Hospital Affiliated to Shandong First Medical University. If necessary, please contact the corresponding author by email (Hengtao Qi, elementfe@126.com).

Received: 10 March 2025; Accepted: 29 October 2025
Published online: 17 November 2025

References

1. AlShareef, S. & Newton, B. W. in *StatPearls* (StatPearls Publishing LLC., 2024).
2. da Silva-Correia, A. G., Alves, J. N., da Mota-Santos, S. A., Guerra, D. R. & Garção, D. C. Anatomical variations in the relationship between the spinal accessory nerve and internal jugular vein: a systematic review and meta-analysis. *Int J Oral Maxillofac Surg* **52**, 13–18. https://doi.org/10.1016/j.ijom.2022.03.008 (2023).
3. Johal, J. et al. The accessory nerve: a comprehensive review of its anatomy, development, variations landmarks and clinical considerations. *Anat Rec (Hoboken)* **302**, 620–629. https://doi.org/10.1002/ar.23823 (2019).
4. Shah, F., Qamar, S. N., Jaffer, M. & Crosbie, R. Dual spinal accessory nerve: an anatomical anomaly during neck dissection. *BMJ Case Rep* https://doi.org/10.1136/bcr-2022-249866 (2023).
5. Suzuki, H., Matsui, Y., Iwai, T., Nishida, M. & Iwasaki, N. Usefulness of ultrasonography for diagnosing iatrogenic spinal accessory nerve palsy after lymph node needle biopsy: a case report. *BMC Musculoskelet Disord* **21**, 712. https://doi.org/10.1186/s12891-020-03737-w (2020).
6. Powell, G. M., Baffour, F. I., Baillargeon, A. M., Spinner, R. J. & Glazebrook, K. N. Preoperative ultrasound accurately characterizes surgically confirmed extracranial spinal accessory nerve injuries. *Skeletal Radiol* **51**, 1179–1188. https://doi.org/10.1007/s00256-021-03945-y (2022).
7. Cesmebasi, A., Smith, J. & Spinner, R. J. Role of Sonography in Surgical Decision Making for Iatrogenic Spinal Accessory Nerve Injuries: A Paradigm Shift. *J Ultrasound Med* **34**, 2305–2312. https://doi.org/10.7863/ultra.15.01049 (2015).
8. Beasley, W. D. & Gibbons, C. P. Cranial nerve injuries and the retrojugular approach in carotid endarterectomy. *Ann R Coll Surg Engl* **90**, 685–688. https://doi.org/10.1308/003588408x318138 (2008).
9. Seror, P. Accessory nerve lesion after cervicofacial lift: clinical and electrodiagnostic evaluations of two cases. *Muscle Nerve* **39**, 400–405. https://doi.org/10.1002/mus.21165 (2009).
10. Kim, D. H., Cho, Y. J., Tiel, R. L. & Kline, D. G. Surgical outcomes of 111 spinal accessory nerve injuries. *Neurosurgery* **53**, 1106–1112. https://doi.org/10.1227/01.neu.0000089058.82201.3d (2003).
11. Aksoy, I. A., Schrader, S. L., Ali, M. S., Borovansky, J. A. & Ross, M. A. Spinal accessory neuropathy associated with deep tissue massage: a case report. *Arch Phys Med Rehabil* **90**, 1969–1972. https://doi.org/10.1016/j.apmr.2009.06.015 (2009).
12. Gun, K. et al. Spinal accessory nerve injury: eight cases and review of the literature. *Clin Ter* **165**, 211–216. https://doi.org/10.7417/ct.2014.1736 (2014).
13. Lucchetta, M. et al. Nerve ultrasound findings in two cases of spinal accessory nerve palsy. *Muscle Nerve* **49**, 293–294. https://doi.org/10.1002/mus.24083 (2014).

14. Camp, S. J. & Birch, R. Injuries to the spinal accessory nerve: a lesson to surgeons. *J Bone Joint Surg Br* **93**, 62–67. https://doi.org/10.1302/0301-620x.93b1.24202 (2011).
15. Ricci, V. et al. Histopathology and high-resolution ultrasound imaging for peripheral nerve (injuries). *J Neurol* **269**, 3663–3675. https://doi.org/10.1007/s00415-022-10988-1 (2022).
16. Hung, C. Y. et al. Pictorial essay on ultrasound and magnetic resonance imaging of paraspinal muscles for myofascial pain syndrome. *Life (Basel)* https://doi.org/10.3390/life14040499 (2024).
17. Chang, K. V. et al. Sonographic Nerve Tracking in the Cervical Region: A Pictorial Essay and Video Demonstration. *Am J Phys Med Rehabil* **95**, 862–870. https://doi.org/10.1097/phm.0000000000000557 (2016).
18. Meng, S., Platzgummer, H., Loizides, A., Chang, K. V. & Gruber, H. Ultrasound of Small Nerves. *Ultraschall Med* **43**, 12–33. https://doi.org/10.1055/a-1495-5294 (2022).
19. Ricci, V. & Özçakar, L. Ultrasound imaging of the upper trapezius muscle for safer myofascial trigger point injections: a case report. *Phys Sportsmed* **47**, 247–248. https://doi.org/10.1080/00913847.2019.1589105 (2019).
20. Laughlin, R. S., Spinner, R. J. & Daube, J. R. Electrophysiological testing of spinal accessory nerve in suspected cases of nerve transection. *Muscle Nerve* **44**, 715–719. https://doi.org/10.1002/mus.22135 (2011).
21. Walter, U. How small can small nerves be for diagnostic ultrasonography?. *Ultraschall Med* **40**, 400–402. https://doi.org/10.1055/a-0961-3487 (2019).
22. Canella, C. et al. Anatomical study of spinal accessory nerve using ultrasonography. *Eur J Radiol* **82**, 56–61. https://doi.org/10.1016/j.ejrad.2011.04.038 (2013).
23. Hong, M. J. et al. Spinal Accessory Nerve: Ultrasound Findings and Correlations with Neck Lymph Node Levels. *Ultraschall Med* **37**, 487–491. https://doi.org/10.1055/s-0034-1385673 (2016).
24. Casaletto, E. et al. Ultrasound imaging of nerves in the neck: Correlation with MRI, EMG, and clinical findings. *Neurol Clin Pract* **10**, 415–421. https://doi.org/10.1212/cpj.0000000000000767 (2020).
25. Silkjær-Bak, S., Johnsen, B., Fuglsang-Frederiksen, A., Døssing, K. & Qerama, E. Comparison of ultrasound with electrodiagnosis of scapular winging: A prospective case control study. *Clin Neurophysiol* **133**, 48–57. https://doi.org/10.1016/j.clinph.2021.09.021 (2022).
26. Ricci, V. et al. Ultrasound imaging and guidance for cervical myofascial pain: a narrative review. *Int J Environ Res Public Health* https://doi.org/10.3390/ijerph20053838 (2023).
27. Townsley, P., Ravenscroft, A. & Bedforth, N. Ultrasound-guided spinal accessory nerve blockade in the diagnosis and management of trapezius muscle-related myofascial pain. *Anaesthesia* **66**, 386–389. https://doi.org/10.1111/j.1365-2044.2011.06691.x (2011).
28. Silkjær-Bak, S., Johnsen, B., Fuglsang-Frederiksen, A., Døssing, K. & Qerama, E. Neuromuscular ultrasound of the scapular stabilisers in healthy subjects. *Clin Neurophysiol Pract* **6**, 72–80. https://doi.org/10.1016/j.cnp.2021.01.003 (2021).
29. Fu, S., Xue, G., Jiang, L., Xue, H. & Cui, L. High-Resolution Ultrasound Imaging of Axillary Nerve and Relevant Injury. *J Ultrasound Med* **42**, 2115–2123. https://doi.org/10.1002/jum.16233 (2023).
30. Lung, K. & Lui, F. in *StatPearls* (StatPearls Publishing LLC., 2024).
31. Tessler, J. & Talati, R. in *StatPearls* (StatPearls Publishing LLC., 2024).
32. Glover, N. M., Black, A. C. & Murphy, P. B. in *StatPearls* (StatPearls Publishing LLC., 2024).
33. Zeidenberg, J., Burks, S. S., Jose, J., Subhawong, T. K. & Levi, A. D. The utility of ultrasound in the assessment of traumatic peripheral nerve lesions: report of 4 cases. *Neurosurg Focus* **39**, E3. https://doi.org/10.3171/2015.6.Focus15214 (2015).
34. Nwawka, O. K. Ultrasound Imaging of the Brachial Plexus and Nerves About the Neck. *Ultrasound Q* **35**, 110–119. https://doi.org/10.1097/ruq.0000000000000396 (2019).
35. Shen, J. et al. Ultrasound in the management of iatrogenic spinal accessory nerve palsy at the posterior cervical triangle area. *Muscle Nerve* **59**, 64–69. https://doi.org/10.1002/mus.26342 (2019).

Author contributions

Research conception and design: Hengtao Qi; Data acquisition: Zijian Tai, Lihua Liu, Tiezheng Wang and Hengtao Qi; Statistical analysis: Zijian Tai, Yeting Wang, Hengtao Qi and Lihua Liu; Data analysis and interpretation: Zijian Tai, Hengtao Qi and Lihua Liu; Drafting of the manuscript: Zijian Tai, Lihua Liu and Tiezheng Wang; Critical revision of the manuscript: Kezhen Qin, Wen Chen and Huawei Zhang; Technical, or material support: Kezhen Qin, Wen Chen and Huawei Zhang; Supervision: Zijian Tai, Lihua Liu, Tiezheng Wang and Hengtao Qi. All authors reviewed the manuscript. Approval of the final manuscript: All authors.

Declarations

Competing interests

The authors declare no competing interests.

Ethical approval

All procedures performed in studies involving human participants were in accordance with the ethical standards of the institutional research committee and with the 1964 Helsinki declaration and its later amendments or comparable ethical standards.

Informed consent

All volunteers and patients provided written informed consent.

Additional information

Supplementary Information The online version contains supplementary material available at https://doi.org/10.1038/s41598-025-26644-3.

Correspondence and requests for materials should be addressed to H.Q.